

Investigations on the characterization of laminar and transitional flow conditions after high pressure homogenization orifices

Katharina Kelemen · F. E. Crowther ·
C. Cierpka · L. L. Hecht · C. J. Kähler ·
H. P. Schuchmann

Received: 25 April 2014 / Accepted: 1 July 2014 / Published online: 10 July 2014
© Springer-Verlag Berlin Heidelberg 2014

Abstract High pressure homogenization is a well-established technique to achieve droplets in the submicron range. However, droplet breakup mechanisms are still not completely understood, since studies to characterize the flow are limited due to very small dimensions (typically several micrometers) and very large velocity ranges (from almost stagnant flow to 300 m/s and more). Furthermore, cavitation can occur resulting in multiphase flow. So far, experiments were performed only via integral measurements of, for example, the pressure drop or the droplet size distribution at the outlet. In the current study, this gap shall be closed using Particle Image Velocimetry measurements to analyze the flow field. In addition, an overall method, the characteristic correlation between the discharge coefficient (C_D) and $Re^{0.5}$ is used to distinguish between laminar, transitional and turbulent flow conditions at Reynolds numbers based on the channel width ($d = 200 \mu\text{m}$) between 250 and 22,500. The investigated orifices of this study had different positions of the constriction: coaxial and next to the wall. For both orifices, the C_D measurement was applicable and showed different characteristic regions which can be associated with laminar, transitional and turbulent flow conditions. Mean velocity fields and fluctuations were measured quantitatively at the outlet and 50

diameters downstream using Micro Particle Image Velocimetry (μ -PIV) in an optically accessible orifice. Increased velocity fluctuations were found in the shear layers when the flow turns from laminar into unstable transitional conditions. The combination of both measurement techniques will help to optimize these systems for the future.

Keywords High pressure homogenization · Discharge coefficient · Orifice · μ PIV

List of Symbols

A [–]	Cross-sectional area of the orifice
B [mm]	Width of the squared orifice
B [mm]	Width of the squared inlet and outlet of the orifice unit
C_D [–]	Discharge coefficient
$C_{D,\text{const}}$ [–]	Constant discharge coefficient
D [mm]	Diameter of the orifice
D [mm]	Diameter of the inlet and outlet of the orifice unit
d/D [–]	Ratio of orifice diameter to outlet diameter
h [mm]	Step height of a backward facing step
H [mm]	Outlet height of a backward facing step
L [mm]	Length of the orifice
N_{total} [–]	Number of images
N_{vector} [–]	Number of vectors accounting for calculation
Δp [bar]	Homogenization pressure
Δp_I [bar]	Pressure loss after the first orifice unit
Δp_{ideal} [bar]	Frictionless pressure loss
Δp_{max} [bar]	Maximum pressure loss
Δp_{real} [bar]	Real pressure loss
Δp_{total} [bar]	Total homogenization pressure
Re [–]	Reynolds number

K. Kelemen (✉) · F. E. Crowther · L. L. Hecht ·
H. P. Schuchmann

Institute of Process Engineering in Life Sciences Section I:
Food Process Engineering, Karlsruhe Institute of Technology,
Kaiserstr. 12, 76131 Karlsruhe, Germany
e-mail: Katharina.Kelemen@kit.edu

C. Cierpka · C. J. Kähler
Institute of Fluid Dynamics and Aerodynamics, Universität der
Bundeswehr München, Werner-Heisenberg-Weg 39,
85577 Neubiberg, Germany

Δt [s]	Interframing time between two images
u [m/s]	Mean axial velocity
u_b [m/s]	Mean bulk velocity
$u_{\text{exit},c}$ [m/s]	Mean exit centerline velocity
$u_{m,c}$ [m/s]	Mean centerline velocity
$u'^2/u_{m,c}^2$ [-]	Normalized Reynolds shear stresses axial direction
$v'^2/u_{m,c}^2$ [-]	Normalized Reynolds shear stresses radial direction
\dot{V} [m ³ /s]	Volume flow rate
x [mm]	Streamwise or axial coordinate
x/d or x/b resp.	Normalized distance after the orifice
y [mm]	Lateral or radial coordinate
y/d or y/b resp.	Normalized diameter of the orifice
z	Height coordinate

Greek letters

η [mPa s]	Dynamic viscosity of the fluid
ρ [kg/m ³]	Density of the fluid
cp	Counter pressure
μ -PIV	Micro Particle Image Velocimetry
PEG	Polyethylene glycol

1 Introduction

In high pressure homogenization, emulsions are forced through narrow micro structured devices under high pressure ($\Delta p = 300$ – $2,000$ bars) in order to break up the droplets. Simple orifices can be used to achieve droplet sizes in the range of 0.4 – $5 \mu\text{m}$ (Stang et al. 2001). The orifice diameter is typically in the range of 80 – $200 \mu\text{m}$. Due to the high pressure, strong gradients and thus stresses in the flow are produced. Stresses resulting from elongational and shear gradients or developing vortices in the fluid disrupt the droplets, if they are applied by a certain extent and for a certain time. The mechanisms of the droplet breakup are known to depend on the flow conditions. In well-defined flow patterns such as laminar shear or elongational flows, the droplet breakup has been studied intensively over the past decades. In fully developed turbulent conditions, there are also approaches to describe the droplet breakup with respect to the size of vortices compared to the droplet. In such defined flows, it has been shown that the maximum droplet size which is not disrupted can be further associated with the energy input (Hinze 1955; Kolmogorov 1958; Grace 1982; Karbstein 1994).

However, in high pressure homogenization, different fluctuating and overlapping flow conditions are present simultaneously. First, the flow is accelerated to several 100 m/s within milliseconds due to the sudden reduction of

the cross-sectional area, causing elongational flow at the inlet.

At the outlet of the small channel, a jet with a very thin shear layer forms. This jet tends to bend toward one wall. The preferred position might change for subsequent experiments. However, the jet remains attached to either wall for the rest of the experiment and a recirculation regions forms. The flow field therefore features a high dynamic spatial range and a very high dynamic velocity range from high-speed channel flow to almost stagnant regions. Depending on the velocity, the jet reattaches to the wall in laminar flow conditions, but develops instabilities with increasing velocity until the transition to full turbulence takes place. Due to these complex flow features, the models describing the final droplet size are only of limited applicability. The characterization of the flow conditions in high pressure homogenization devices depending on process parameters is thus crucial for the prediction of the resulting droplet size.

The classification of flow conditions has been studied for more than a century. The distinction between laminar and turbulent flow was first visualized by Reynolds in 1883 (Reynolds 1883) and is also applicable in this case. The *Reynolds Number*

$$\text{Re} = \frac{\rho u_b d}{\eta} \quad (1)$$

is built with the density of the fluid ρ , the bulk velocity u_b , the diameter of the orifice d , and the dynamic viscosity of the fluid η . Pipe flows are considered to be laminar when $Re_{\text{crit}} < 2,300$ and fully turbulent when $Re > 10^5$. Between these values, the flow is considered to be in transition. However, disturbances such as wall roughness, restrictions or curves can influence Re_{crit} . Another dimensionless parameter, the discharge coefficient (C_D value) can be applied to describe the flow conditions downstream from the orifices. The C_D value is defined as the square root of the ratio of ideal, incompressible, frictionless pressure loss Δp_{ideal} to the real pressure loss Δp_{real} :

$$C_D = \sqrt{\frac{\Delta p_{\text{ideal}}}{\Delta p_{\text{real}}}} = \frac{\dot{V}}{A} \sqrt{\frac{\rho(1 - (d/D)^4)}{2\Delta p}} \quad (2)$$

with the volume flow rate \dot{V} , the cross-sectional area of the orifice A , the ratio of orifice diameter to outlet diameter d/D and the measured pressure loss Δp .

The trend of the C_D value vs. $Re^{0.5}$ downstream from an orifice was correlated with flow visualizations by Johansen in 1930. He distinguished between laminar, transitional and turbulent flow from the course of the graph: Under laminar flow conditions, the C_D is proportional to $Re^{0.5}$. With increasing Re , the C_D value reaches a maximum. At this point, first instabilities in the shear layer of the jet indicate

the transitional flow, which still reattaches to the wall after the orifice and returns to the original laminar flow pattern. The C_D value decreases with further increase of Re until a constant C_D value, independent of Re , is reached. This is attributed to turbulent conditions since the boundary layer does not change anymore (Johansen 1930). The exact slope of the curve of the C_D value is strongly influenced by the geometry of the orifice (Lichtarowicz et al. 1965; Tunay et al. 2004).

Using this method, the flow of emulsions was investigated through an orifice under laminar, transitional and turbulent conditions. Furthermore, the disruption of these emulsions has been investigated under varying flow conditions. The obtained mean droplet sizes could be correlated with the present flow conditions determined by the shape of the C_D curve (Wolf et al. 2012; Kelemen et al. 2014).

However, this method can only give an estimate of the overall flow conditions and does not show the transition on a local scale nor the spatial extent of it. Stresses which contribute to the droplet breakup on a local scale cannot be resolved.

Measurement techniques, such as pitot-static systems or hot-film anemometry, which measure the velocity at a fixed location with high temporal resolution, can be used for the acquisition of information on velocity and fluctuations in velocity over time (Ball et al. 2012). These measurement techniques have been used since the 1930s for the investigation of macroscopic free jets emerging from small holes or slits in quiescent fluid for both laminar (Schlichting 1933) and turbulent (Tollmien 1926) flow conditions but cannot be used in micro channels due to their invasive character. Most of the investigations focus on completely turbulent jets with $Re > 10,000$. Recently, Ball et al. (2012) gave a comprehensive review on the characterization of the turbulent round free jet describing the influences of *Reynolds* Number and inlet conditions on the developing jet. In classical theory, a jet can be classified in the near-field region behind the exit until about 7 diameters distance ($x/d \leq 7$), the intermediate field and the far-field region ($x/d \geq 70$) (Ball et al. 2012). The flow structure of free jets is different than the one of confined jets, as found in homogenization devices. However, the characteristics of the flow in the near field close to the orifice exit are comparable (Singh et al. 2003). The development of the shear layer of the jet leading to turbulent transition in the far field is strongly dependent on the orifice shape. The velocity decay and turbulent intensities are affected if the shape is not axially symmetric (elliptical or triangular shape). Circular, squared or even cross-shaped orifices show fewer differences (Singh et al. 2003; Mi and Nathan 2010).

To investigate the complete velocity field in order to calculate stresses and turbulent quantities on a local scale,

measurement techniques with high spatial resolution are necessary. Particle Image Velocimetry (PIV) is such a technique. The flow of interest is seeded with small tracer particles that should faithfully follow the flow. The particles are then illuminated by a light source (typically a double pulse laser), and two successive images of the particle distribution are taken. The velocity field is calculated, based on the cross-correlation between these images. PIV has already been used to quantify the instabilities in the shear layer of macroscopic turbulent free jets by elaborating on the maximum fluctuations of the velocity. The values of the Reynolds normal and shear stresses show a peak at the exit of the orifice in the shear layer and are smoothed out over the whole jet downstream, as it is decelerated (Galinat et al. 2007; Mi et al. 2007; Milanovic und Hammad 2010).

For flow characterization on small scales ($d < 1$ mm) μ -PIV has been adapted from PIV (Santiago et al. 1998). Due to limitations of the magnification and technically the possible minimal time separation between two images of the camera, there are certain limitations regarding the velocity which can be measured. Thus, applications of μ -PIV on high speed and turbulence investigations are rare. The spatial resolution for μ PIV is very high. However, due to the cross-correlation of interrogation windows of certain size, the smallest scales cannot be resolved for high Re flows. Due to the volume illumination also out of focus particle contribute to the correlation signal and thus the velocity is also depth averaged. However, both effects can be minimized using window deformation and proper image preprocessing (Rossi et al. 2012).

Using a μ -PIV setup Blonski et al. measured the velocity through a gap of 400 μm of up to 25 m/s and found the highest turbulent kinetic energy in the shear layer right at the exit (Blonski et al. 2007). Velocities of up to 300 m/s were measured by Gothsch et al. in cooperation with the Bundeswehr University Munich in a microfluidic dispersing device ($d = 80 \mu\text{m}$) with a setup of two cameras (Gothsch et al. 2014). In principle, the technique worked very well; however, there are a lot of challenges to address. Currently, this case of a high-speed micro scale flow is therefore subject of the 4th PIV challenge, where developers of the technique qualify their latest codes. To characterize the flow on a small scale at high pressure, as it is the case in high pressure homogenization, the optical access is very challenging. This is why several investigators do not measure at a scale of 1:1, but instead scale up their models to larger sizes (Innings and Trägårdh 2007). It is possible to scale up the droplet breakup by keeping the relevant dimensionless numbers constant (Innings et al. 2011). However, it only applies for non-cavitating systems without any surfactants, since these timescales cannot be scaled. It is not yet clarified if the findings from large scale

system can be adapted completely to droplet breakup in homogenizers at microscale.

To our knowledge, the flow characterization in high pressure homogenization devices at transitional flow conditions has not been published in detail so far. Laminar and turbulent conditions are described fairly well for similar geometries; however, in high pressure homogenization, turbulent conditions are often not reached, due to the high viscosity of the processed emulsions. Therefore, the transitional flow regime, where a laminar jet undergoes instabilities, is of high interest.

As outlined above, two different methods to describe the flow downstream from a high pressure orifice were applied for the current investigation:

C_D measurements were used to estimate the flow regime. This method is very practical to apply to any running high pressure homogenization process and gives first hints about the flow conditions. Furthermore, the local flow and the turbulent quantities were obtained via μ PIV at different laminar and transitional process conditions.

1.1 Experimental details

The high pressure setup used for both flow characterization methods is depicted in Fig. 1. It consists of a pressure vessel (I) with a $\Delta p_{\max} = 100$ bars and the orifice units (II and III). Two different modes of operation were investigated: A single-step pressure drop, where only orifice 1 (II) is used and a two-step pressure drop, where a second orifice 2 (III) is used to apply a counter pressure (cp) behind orifice 1 of about 15–17.5 % of the total homogenization pressure Δp_{total} . Counter pressure is widely used in emulsification to influence cavitation (Freudig et al. 2003). The flow is driven by applying pressure with a nitrogen gas bottle at homogenization pressures $\Delta p_{\text{total}} = p_0 - p_2$ of 10, 40 and 80 bars. Pressure indicators (PI) monitored the pressure before and after the orifices. The volume flow rate

which was necessary to calculate the C_D value was measured by a Coriolis mass flow indicator (MI) downstream from the orifice.

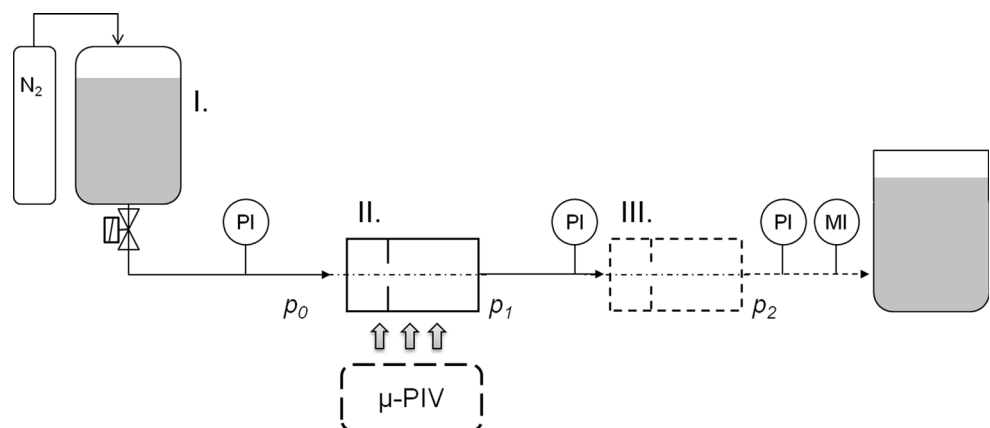
The orifice units used in the current investigation had a right-angle outlet. The publications for these types are seldom since most orifices investigated in the literature are very short and sharp-edged, which means the diameter is 45° bevelled instead of 90° .

The difference between the orifices was the shape of their cross-section, their diameter and the orifice position (see Fig. 2). Orifice unit A had a circular cross-section and was coaxially positioned. The orifice diameter was $d = 200 \mu\text{m}$ with a length of $l = 2$ mm having a conical inlet angle of 59° . The aspect ratio between the small channel and the outlet was 10. Inlet and outlet had a diameter of $D = 2$ mm. Both orifices had an inlet and outlet length of 30 mm. Orifice unit A was drilled into steel and fixed with steel blocks. A similar orifice unit with different dimensions ($d = 300 \mu\text{m}$, $l = 1$ mm, $D = 2$ mm) was used as orifice 2 if counter pressure after orifice 1 was applied.

To realize the optical flow investigations via μ PIV, the orifice unit was modified. Orifice unit B was made of a steel block, where the channel is machined in. It was covered with optical-grade PMMA glass plate and sealed. Therefore, the reduction in the cross-sectional area of the channel is positioned next to the upper glass plate (see Fig. 2). The squared orifice width was $b = 200 \mu\text{m}$ which results in the same hydraulic diameter as the circular orifice 1 in unit A. The length was $l = 3$ mm and the squared inlet and outlet channel width was $B = 2$ mm.

For the investigation of the flow at different dynamic viscosities η , demineralized water was thickened with polyethylene glycol of molar mass $M = 20,000$ g/mol (PEG 20,000 ROTIPURAN[®]; Carl Roth GmbH + Co. KG). Two PEG solutions were prepared with $\eta = 12.5$ mPa s (10 % w/w) and $\eta = 5.4$ mPa s (6 % w/w), respectively. Dynamic viscosities were measured with a Couette geometry of a

Fig. 1 Experimental setup with pressure vessel (I) and the orifices (II and III)



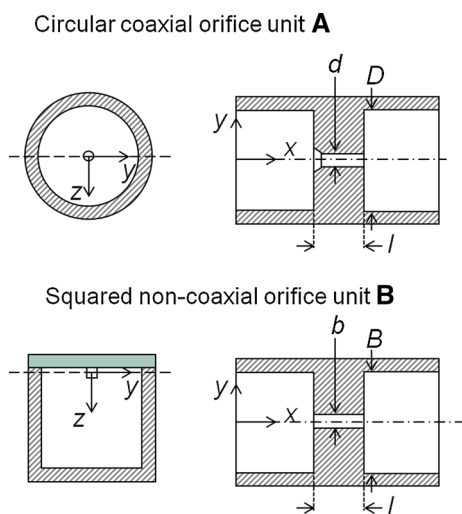


Fig. 2 Shape and scale of orifice unit A and B

rotational rheometer (Anton Paar Physica MCR 30) at shear rates ranging from 1 to $5 \cdot 10^5 \text{ s}^{-1}$ at 25 °C. In this range, the solution is characterized by Newtonian flow behavior.

1.2 C_D measurements

Volume flow rate \dot{V} and pressure before (p_0) and after (p_1) orifice 1 were measured simultaneously for demineralized water as well as the two PEG solutions. The C_D value was then calculated from \dot{V} , $\Delta p_1 = p_0 - p_1$ and the orifice dimensions. Δp_1 was varied between 5 and 90 bars leading to a volume flow from 0.02 to 0.2 L/min.

1.3 μ PIV measurements

The PEG solutions were seeded with 1.1 μm polystyrene particles coated with the fluorescent dye Nile red (Fluorospheres, Invitrogen, USA). The correct concentration of the seeding solution can be estimated from the depth of correlation (DOC) and the desired final interrogation window size (Keane and Adrian 1990; Olsen and Adrian 2000). The DOC corresponds to the volume in which particles are imaged by the camera with significant intensities and therefore contribute to the cross-correlation and thus bias the velocity measurements. Using proper image preprocessing, the DOC can be minimized. However, the theoretical value was estimated to be 46.3 μm at the maximum. The concentration of the seeding particle solution was 0.0025 % w/w to ensure at least 5 particles images in each interrogation volume (Keane and Adrian 1990). At this low concentration, the seeding particles did not have an influence on the dynamic viscosity.

The μ PIV setup features a double-pulsed ND:YAG laser (Dual Power 30.15 of Litron Lasers) operated at a frequency of 8 Hz and attenuated to 30 mJ/pulse with a wavelength of 532 nm. Depending on the flow velocity, the interframing

time Δt between the two pulses was adjusted from 0.2 to 4 μs . The laser beam was directed through an inverted microscope (DM IRM, Leica Microsystems Wetzlar GmbH) and an objective lens into the microchannel. The objective lens (C PLAN by Leica) has a 10 \times magnification and a numerical aperture of $NA = 0.22$. The camera (Hi-Sense Neo sCMOS by Dantec Dynamics) had a CCD chip size of 5.5 Megapixels and 16-bit dynamic range. It was operated at double frame acquisition mode with results in a minimum $\Delta t = 0.12 \mu\text{s}$ between successive frames. The imaged region was approximately $2 \times 2 \text{ mm}^2$ with a final magnification of one pixel corresponding to 1.4 μm .

To reduce the bias by the DOC and enhance the signal to noise ratio images were processed by subtracting a mean image and setting an intensity threshold to minimize errors arising from background noise. A multi-pass cross-correlation algorithm (Dynamic Studio 3.4 by Dantec Dynamics) with window deformation was applied. The interrogation window sizes were decreased in steps from 64×64 pixels to the final resolution of 16×16 pixels to ensure a high resolution at a large velocity range. The final interrogation window size of 16×16 pixels corresponds to $22 \times 22 \mu\text{m}^2$. An overlap of 50 % was used, resulting in a final distance of 11.2 μm between vectors. The vector fields were filtered to remove outliers. These erroneous vectors were removed and are not included in the calculation of the mean velocity fields or Reynolds stresses. For each measurement position, 228 velocity fields were collected, which was the maximum available image number of the μ -PIV system used for this investigation.

Velocity fields were captured at the outlet of the orifice and at three different distances x downstream of the orifice ranging from $x/b = 10$ to 50. At each distance, the velocity was monitored over time at four positions to check whether a stationary velocity was reached within $N_{\text{total}} = 228$. A calculation of the mean velocity is only reasonable if a stationary value is reached in the number of images taken. The number of images until the fluctuations are $< \pm 0.3 \%$ of the mean flow velocity is summarized in Table 1 for the

Table 1 Number of images taken until the deviation in stationary velocity is smaller than 0.3 %

$\eta = 12.5 \text{ mPa s}$	Outlet	Downstream		
		$x/b = 10$	$x/b = 25$	$x/b = 40$
$\Delta p_{\text{total}} = 10 \text{ bars}$	170	200	160	180
$\Delta p_{\text{total}} = 40 \text{ bars}$	190	–	–	–
$\Delta p_{\text{total}} = 80 \text{ bars}$	200	–	–	–
$\Delta p_{\text{total}} = 10 \text{ bars (c.p.)}$	200	180	200	220
$\Delta p_{\text{total}} = 40 \text{ bars (c.p.)}$	180	210	–	–
$\Delta p_{\text{total}} = 80 \text{ bars (c.p.)}$	200	–	–	–

Mean value of four positions at each location

flow with $\eta = 12.5$ mPa s. At the outlet and at $\Delta p_{\text{total}} = 10$ bars, the number of images taken was enough to be representative for the mean flow. At higher homogenization pressures, the difference from the mean field was $> \pm 0.5$ %. However, with the current setup, only 228 images could be taken at this high resolution.

2 Results and discussion

2.1 Characterizing the integral flow conditions via C_D measurements

The C_D measurements were carried out with orifice unit A and B in order to investigate whether the position of the orifice influences the applicability of the measurement technique. The shape of the orifices was different (circular and squared, same hydraulic diameter). This fact has been neglected in the following discussion, since it has been shown that the shape of axisymmetric orifices has no significant influence on the maximum velocity and turbulent intensities downstream of the orifice (Mi and Nathan 2010).

For each orifice unit, the C_D value was captured at different $Re^{0.5}$. Three fluids with different dynamic viscosities of $\eta = 0.9, 5.4$ and 12.5 mPa s were used. In this way, a total range of Reynolds Numbers from 250 to 22,500 could be realized within $\Delta p_{\text{max}} = 100$ bars. This method has been used by several investigators before (Johansen 1930; Bogema and Monkmeyer 1960).

The resulting C_D value over $Re^{0.5}$ measured in the coaxial orifice unit A is depicted in Fig. 3. In the range of $Re^{0.5} = 22 \dots 400$ ($Re = 480 \dots 16,000$), the measurement points fall on top of each other for $\eta = 5.4$ and 12.5 mPa s. The main characteristics of the curve as described in the literature are reproduced well: At the lowest Reynolds Number (obtained with $\eta = 12.5$ mPa s), a linear increase of the C_D value indicates laminar flow conditions after the orifice. At $Re^{0.5} > 25$ ($Re > 630$), the curve bends and the slope flattens until a maximum is reached at about $Re^{0.5} = 62$ ($Re = 3,800$). This maximum indicates the state where the instabilities in the shear layer are not damped to result in laminar flow downstream but turbulence is produced (Johansen 1930; Tunay et al. 2004). A constant C_D value independent of $Re^{0.5}$ is reached with demineralized water ($\eta = 0.9$ maps) at about $Re^{0.5} > 120$ ($Re > 14,400$). This state is attributed to completely turbulent flow.

Figure 4 shows the C_D measurements obtained from orifice unit B. At $Re^{0.5} < 62$ ($Re < 3,800$), the results are similar to those found in the coaxial orifice: First, the C_D value increases linearly before the slope flattens. The measurement points for the viscosities of $\eta = 5.4$ and 12.5 mPa s also agree well. However, there is no clear

maximum to be found in the curve. The maximum in the C_D curve describes the reattachment of the relaminarized jet. Since orifice unit B is not coaxial, a wall jet develops after the orifice which might fluctuate in z -direction since it is influenced by the wall. Investigations on the influence of the ratio of length to diameter l/d on the course of the C_D curve showed that the characteristic peak diminishes with increasing l/d (Lichtarowicz et al. 1965). A constant C_D value is reached at $Re^{0.5} > 120$ ($Re > 14,400$).

Additionally, the C_D value was measured with counter pressure. The obtained results are depicted as hollow symbols in the diagram and there is no influence of the counter pressure on the shape of the curve.

There are a few outliers at very low volume flow rates which are attributed to difficulties to measure flow rates at these conditions.

For both orifice units, the slope of the linear increase and $C_{D,\text{const}}$ were calculated and presented in Table 2. The values are in the same range and it can be concluded that the flow visualization in the orifice unit B with optical access reproduces the behavior within the circular orifice

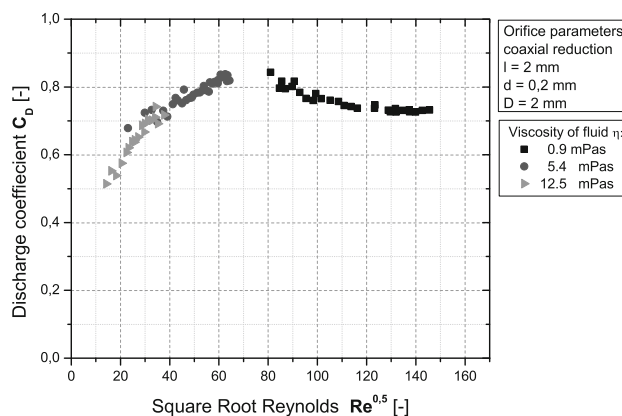


Fig. 3 C_D value as a function of $Re^{0.5}$ of coaxial orifice unit A

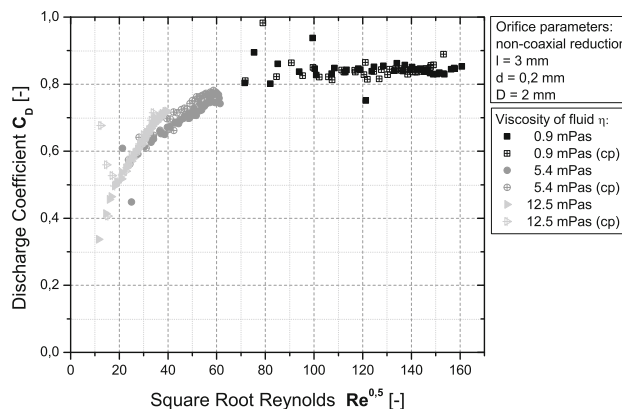


Fig. 4 C_D value as a function of $Re^{0.5}$ of non-coaxial orifice unit B

without optical access. The slope of the linear increase of orifice unit A and B is depicted in Fig. 5 and compared with sharp-edged orifices of various l/d found in the literature. With increasing proportional length of the orifice, the pressure loss coefficient increases. This is inversely proportional to the C_D value; therefore, the slope flattens with increasing l/d . However, orifice unit A is not sharp-edged, but has a conical entrance leading to different behavior of the flow especially in the entrance region. The flow does not detach as in sharp-edged orifices. Both orifices are in fairly good agreement with the literature data. Figure 6 shows the $C_{D, const}$ value of orifice unit A and B as well as several sharp-edged orifices from the literature (Lichtarowicz et al. 1965). $C_{D, const}$ of orifice unit A agrees well with the literature data and is within the region of all the other orifices investigated. Orifice unit B is longer and its $C_{D, const}$ is much lower than the predicted value. However, there are no other orifices of this extended length and the non-coaxial position may influence the $C_{D, const}$ as well.

In both orifice units, it is possible to determine between laminar and turbulent flow conditions. However, the C_D

Table 2 Slope of the linear increase and $C_{D, const}$, for both orifice units with range of $Re^{0.5}$ and error coefficient R^2 of the linearly fitted data

	Linear increase			$C_{D, const}$		
	Slope	Range ($Re^{0.5}$)	R^2	Value	Range ($Re^{0.5}$)	R^2
Coaxial orifice	0.011	14–27	0.96	0.73	>125	0.99
Non-coaxial orifice	0.014	13–25	0.95	0.66	>120	0.99

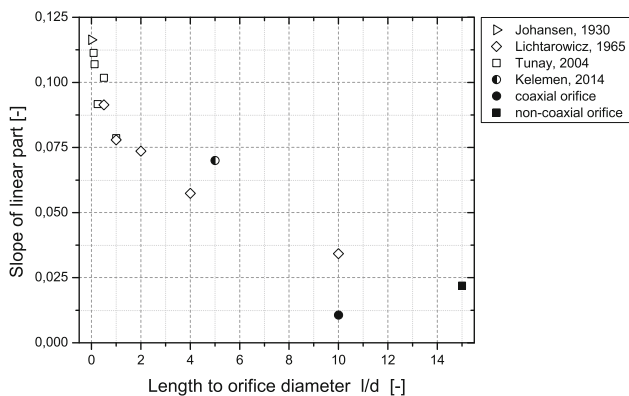


Fig. 5 Slope of the linear part of the C_D curve of orifice unit A and B as well as several sharp-edged orifices from the literature (Johansen 1930; Lichtarowicz et al. 1965; Tunay et al. 2004; Kelemen et al. 2014)

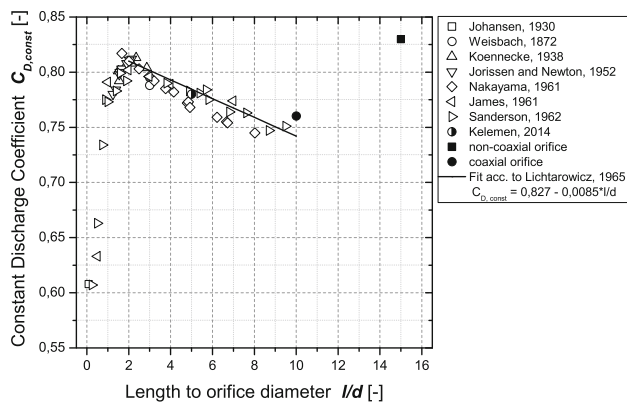


Fig. 6 $C_{D, const}$ of orifice unit A and B in comparison to sharp-edged orifices from the literature (Lichtarowicz et al. 1965; Kelemen et al. 2014)

value can only describe the overall flow type and does not show where and to which extent the flow transitions nor give an idea about local stresses resulting from this.

2.2 μ PIV measurements

2.2.1 Position of the orifice

For all local flow investigations via μ PIV orifice unit B was used, with a non-coaxial reduction in cross-sectional area next to the glass cover (see Fig. 2).

The mean velocity flow fields of the 12.5 mPa s PEG solution at two different homogenization pressures with counter pressure are presented in Fig. 7 ($\Delta p_{total} = 10$ bars) and Fig. 8 ($\Delta p_{total} = 80$ bars), respectively. The mean velocity of the developing jet downstream of the orifice is shown by the vectors (black) and magnitude contours (colored) between $x/b = 0$ and $x/b = 50$ split in four different measurement sections.

At $\Delta p_{total} = 10$ bars (Fig. 7), the mean flow spreads out axisymmetrically in the x - y plane.

At a higher homogenization pressure of $\Delta p_{total} = 80$ bars, the jet is not axisymmetric anymore, but bends slightly toward one wall. This “affinity” to one wall has been observed before by Gothsch et al. in a microchannel after a restriction at turbulent conditions. They saw an attachment of the jet to the wall either to the left or to the right side (Gothsch et al. 2014). In the present investigation, the jet always bends to one side, which might be due to slight inaccuracies in the manufacturing of the orifice unit.

A recirculation area appears from $x/b > 6$ and is stretched out over the whole channel width in the measurement plane at $x/b > 40$. Note that in the downstream measurement sections ($x/b > 10$), the stationary velocity ($\pm 0.3\%$ criteria) was not reached for 228 images (compare Table 1). However, all 228 images are taken into account

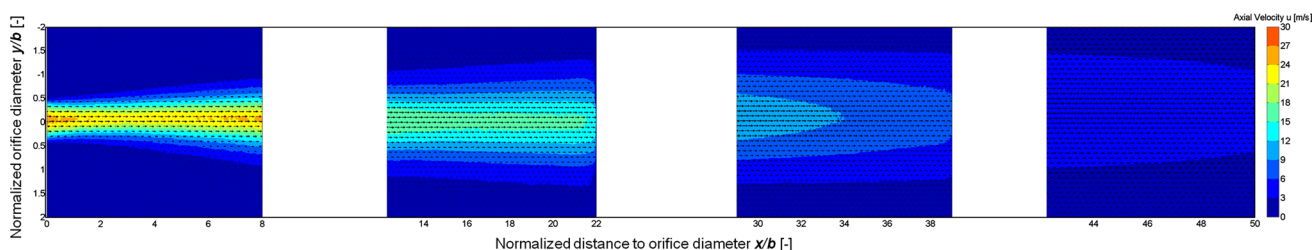


Fig. 7 Mean velocity field of the area after the orifice at $\Delta p_{\text{total}} = 10$ bars with counter pressure ($Re = 330$)

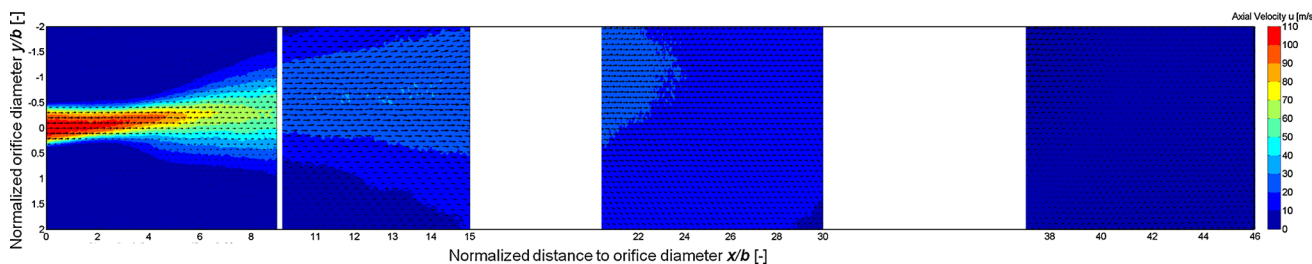
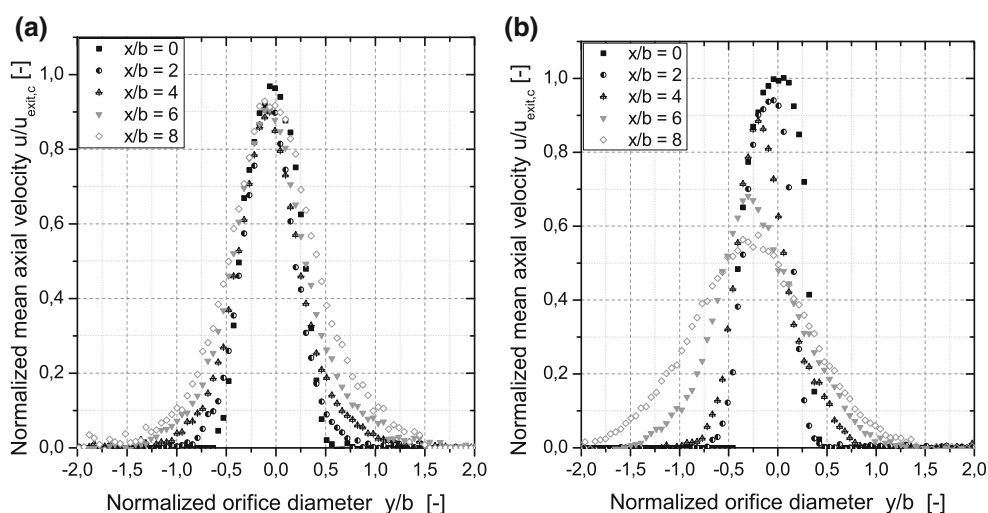


Fig. 8 Mean velocity field of the investigated area at $\Delta p_{\text{total}} = 80$ bars with counter pressure ($Re = 1,280$)

Fig. 9 Axial velocity u at different distances downstream of the orifice: $x/b = 1, 2.5$ and 5 for $\eta = 12.5$ mPa s:

a $\Delta p_{\text{total}} = 10$ bars (incl. counter pressure) and
b $\Delta p_{\text{total}} = 80$ bars (incl. counter pressure)



but the flow conditions can only be described qualitatively. The recirculation region is also known as “roof eddy” in backward facing step geometries (Armaly et al. 1983). In this basic configuration, the expansion of the step is spread over the whole width. Position and length of the roof eddy increase with increasing $Re > 400$ in laminar flow conditions and decrease with transitional conditions until it completely disappears above $Re > 6,000$ (Armaly et al. 1983). The critical *Reynolds* Number at which the roof eddy appears decreases with the expansion ratio of the step height h to the outlet height H (Tihon et al. 2012).

The expansion ratios in all backward facing investigations to our knowledge are $h/H < 3$. The reduction in height in the present investigation is $b/B = 10$. Additionally, the jet expands not only in z -direction but also in the

x - y measurement plane. Therefore, the conditions in the present investigation are rather different and cannot be directly compared to the literature. Nevertheless, the backflow at the higher homogenization pressure $\Delta p_{\text{total}} = 80$ bar and $Re = 1,280$ indicates a roof eddy-like recirculation area.

The following investigations are limited to the measurement position at the outlet since no stationary velocity value could be achieved within $N_{\text{total}} = 228$ at position with $x/b > 8$ (compare Table 1).

To characterize the spreading of the jet in more detail, the profiles of the normalized mean axial velocity $u/u_{\text{exit},c}$ are plotted over the normalized orifice diameter y/b at different distances after the orifice $x/b \leq 8$ (Fig. 9). The orifice extends between $0.5 \leq y/b \leq 0.5$.

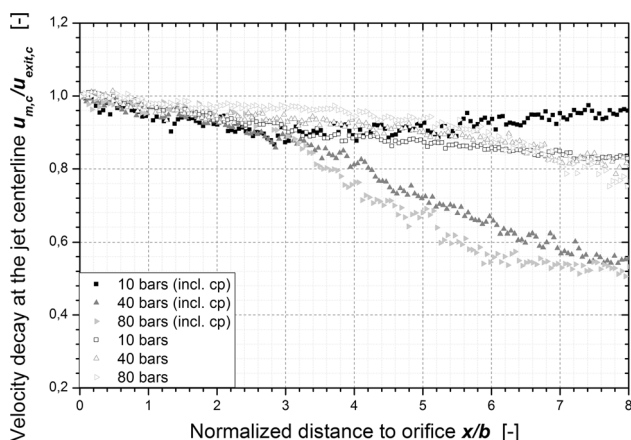


Fig. 10 Velocity decay at the jet centerline $u_{m,c}/u_{exit,c}$ dependent on the normalized distance from the orifice at different homogenization pressures

At $\Delta p_{total} = 10$ bars, the width of the jet increases slightly with the distance. A decrease in the mean velocity is measured at $x/b < 2$, further downstream the mean velocity stays approximately constant. At $\Delta p_{total} = 80$ bars, the width of the profiles stays almost constant until $x/b = 4$ which means the jet spreads with a much slower rate first. Further downstream ($x/b > 4$), the velocity decreases rapidly and the jet widens significantly, which will be discussed further on. A core region of constant axial velocity can also not be seen.

For the process conditions investigated, the development of the velocity after the orifice was quantified by plotting the velocity decay at the jet centerline $u_{m,c}/u_{exit,c}$ over x/b . The jet centerline was defined as the maximum in the profile at each position. Figure 10 shows $u_{m,c}/u_{exit,c}$ of the 12.5 mPa s PEG solution at different homogenization pressures with and without counter pressure. A potential core region where the axial velocity should remain constant cannot be seen and all curves show slight decreases from the exit of the orifice at ($x/b = 0$). Up to $x/b = 2.5$, the velocity at the jet centerline shows a continuous linear decrease indicating a slight deceleration of the flow for all investigated pressures. This behavior is typical for laminar free jets where the mean axial velocity decreases with distance while the jet widens (Pai 1954). At $\Delta p_{total} = 40$ and 80 bars, the decay of the velocity changes abruptly at about $x/b = 3.5$ if counter pressure is applied (filled symbols). In turbulent free jets, the slope of the decay depends on the region: after the potential core or the near-field region. The velocity decreases in the mixing zone due to interactions with the surrounding stagnant fluid which will be entrained in the jet (Ball et al. 2012).

However, no potential core region was detected, and only a change in the decay rate was seen which can be an

indication for a transition to turbulent flow conditions at $\Delta p_{total} = 40$ bars. Hsiao et al. (2010) found the potential core length for turbulent free jets to be 3–4 diameters in right-angled orifices, which matches very well with the significant change in the velocity decay rate in the current investigations.

This significant change in the decay rate for $\Delta p_{total} = 40$ and 80 bars depends on applied counter pressure: With counter pressure the centerline velocity significantly decreases at about $x/b = 3$. If there is no counter pressure this decrease occurs further downstream at about $x/b = 6$.

It can be concluded from Fig. 10 that at $\Delta p_{total} = 10$ bars the development of the jet shows laminar characteristics. At $\Delta p_{total} = 40$ and 80 bars, the flow seems to be still laminar shortly after the orifice, but indicates a mixing zone at $x/b > 3$. Applying counter pressure leads to an earlier decrease of the velocity.

To our knowledge, a similar geometry of a non-coaxial cross-sectional reduction has not been reported in the literature before. Therefore, there is no data to compare the development of the jet centerline and the decay rates and it would be interesting to see if other groups can resemble similar results.

All investigations were realized by measuring the velocity in a xy plane only. Due to the setup, it was not possible to observe the $x-z$ plane. Therefore, it cannot completely be proved, where the jet bends in z -direction. The following investigations regarding the turbulent quantities are therefore limited to the region of $x/b \leq 2.5$ to avoid uncertainties arising from the bending of the jet in either direction.

2.2.2 Turbulent quantities at the outlet of the orifice

To investigate the instabilities in the shear layer of the jet at the exit of the orifice, the normalized velocity fluctuations in axial and radial direction $u'^2/u_{m,c}^2$ and $v'^2/u_{m,c}^2$, respectively, are calculated from the velocity fields. In Fig. 11, they are depicted for 12.5 mPa s PEG solution at $\Delta p_{total} = 10$ and 80 bars including counter pressure (corresponding to the velocity fields in Figs. 7, 8). The fluctuation levels in x -direction are higher than in y -direction and reach up to about 10 % of the mean centerline velocity. At $\Delta p_{total} = 10$ bars (Fig. 11a), corresponding to a low *Reynolds* Number of 330, both $u'^2/u_{m,c}^2$ and $v'^2/u_{m,c}^2$ decrease shortly after the orifice at $x/b < 1$. The fluctuations are evenly distributed over the whole jet diameter without showing peaks. This indicates that the jet shows no shear layer instabilities and remains laminar.

At $\Delta p_{total} = 80$ bars (Fig. 11b) and $Re = 1,280$, a shear layer at around $y/b = \pm 0.5$ depicted by elevated values in both fluctuation levels can be seen. The axial component $u'^2/$

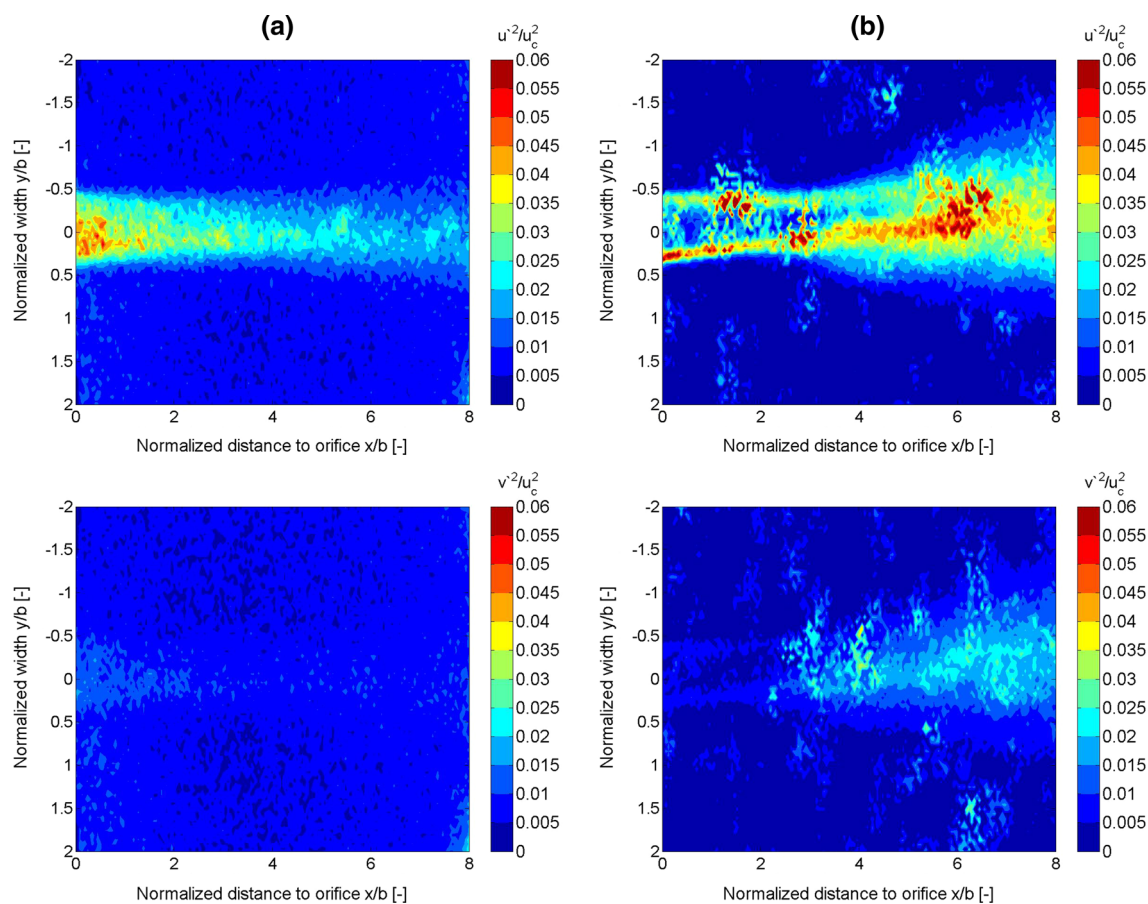


Fig. 11 Contours of the normalized velocity fluctuations $u^2/u_{m,c}^2$ and $v^2/u_{m,c}^2$ obtained between $x/b = 0$ and 8 at **a** $\Delta p_{\text{total}} = 10$ (incl. cp) and **b** $\Delta p_{\text{total}} = 80$ (incl. cp)

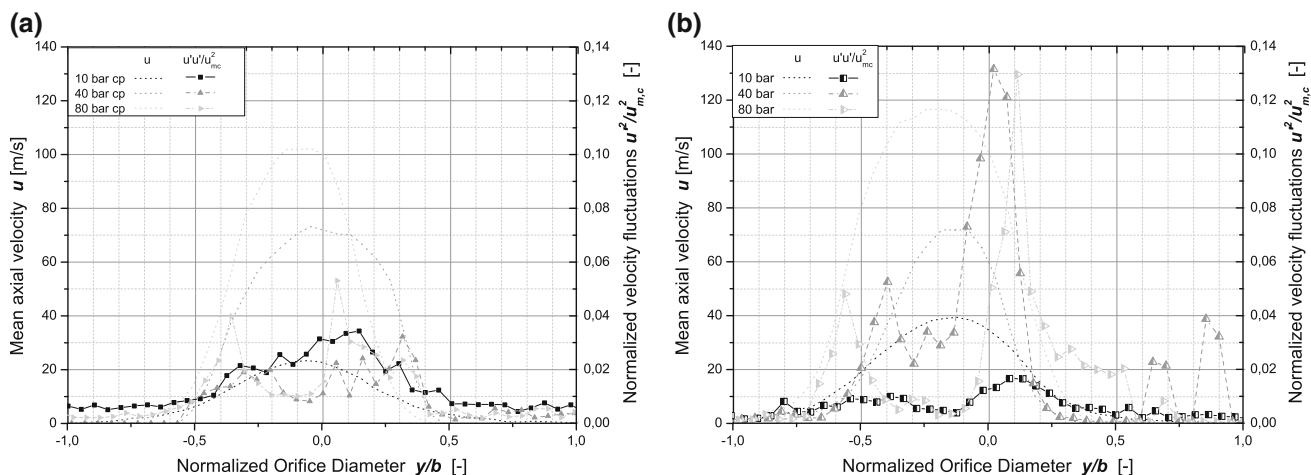


Fig. 12 Axial velocity u and normalized velocity fluctuations $u^2/u_{m,c}^2$ at a constant distance downstream of the orifice $x/b = 2.5$ for $\eta = 12.5$ mPa s at different homogenization pressures $\Delta p_{\text{total}} = 10, 40$ and 80. **a** With counter pressure of 15–17.5 % **b** without counter pressure

$u_{m,c}^2$ shows peaks in the region $x/b < 6$ which widen slightly further downstream. For the radial component $v^2/u_{m,c}^2$, the peaks are not so insignificant at $x/b < 2$, but the absolute levels increase from $x/b > 4$.

To further discuss the turbulent characteristics regarding different homogenization pressures and the impact of counter pressure, radial profiles of the axial fluctuation velocities $u^2/u_{m,c}^2$ are shown for $x/b = 2.5$.

Table 3 Number of vectors accounting for calculation

	Without counter pressure		With counter pressure	
	N_{Vector}	$N_{\text{Vector}}/N_{\text{total}}$	N_{Vector}	$N_{\text{Vector}}/N_{\text{total}}$
10 bars	146	0.63	150.9	0.66
40 bars	67.9	0.30	152.02	0.66
80 bars	89.8	0.39	145.97	0.63

Figure 12a shows $u^2/u_{m,c}^2$ at $\Delta p_{\text{total}} = 10, 40$ and 80 bars including counter pressure. The dotted lines indicate the corresponding axial velocity u . At 10 bars ($Re = 330$) $u^2/u_{m,c}^2$ is distributed over the whole jet as already discussed in Fig. 11. At higher Δp_{total} , $u^2/u_{m,c}^2$ shows peaks at the shear layers of the jet, which are at the radial position where the velocity profile has its biggest gradient. These peaks increase with increasing Δp_{total} from 40 to 80 bars corresponding to $Re = 825$ and 1,280, respectively.

For a comparison without counter pressure, Δp_{total} is now equal to the pressure drop over the orifice investigated and, therefore, higher than in the experiments with counter pressure. This results in higher velocities at each measurement position. The level of $u^2/u_{m,c}^2$ is elevated in the shear layer of the jet for the results without counter pressure. For all homogenization pressures (even at $\Delta p_{\text{total}} = 10$ bars), $u^2/u_{m,c}^2$ has its maxima in the shear layer. With increasing Δp_{total} , the levels of $u^2/u_{m,c}^2$ also rise.

The comparison between Fig. 12a, b suggests that the jet shows higher fluctuations without counter pressure in the shear layer and is therefore more likely for the transition to turbulence further downstream. This could be due to the velocity differences. However, it is more likely that this

effect arises from different flow conditions: if no counter pressure is applied, the flow is more likely to show cavitation in the orifice or shortly behind. Due to a decrease of the local pressures below the saturation pressure vapor cavities grow in the liquid (Brennen 1995). Coalescence of these bubbles lead to areas filled with vapor, where liquid and also seeding particles are lacking. Areas of several interrogation windows with no visible seeding particles appeared in the measurement plane. To estimate the error occurring due to these areas, the number of vectors N_{Vector} available for the calculation of the mean value for of each interrogation window was determined and averaged over the measurement position (see Table 3). When counter pressure was applied (Fig. 12a), 63–66 % of the vectors were valid for processing. This percentage is in a typical range for μPIV [e.g., (Vennemann et al. 2006)]. In the experiments without counter pressure (Fig. 12b), gas bubbles were visible and led to a decrease of the amount of valid vectors which drops below 40 % at $\Delta p_{\text{total}} = 40$ and 80 bars.

It also appears that the occurrence, growth and transportation of gas bubbles lead to an increase in the instabilities in the shear layer.

The influence of the dynamic viscosity of the fluid on the instabilities of the jet is investigated at $\Delta p_{\text{total}} = 40$ bars including counter pressure. Figure 13a, b show the axial velocity as well as $u^2/u_{m,c}^2$ for $\eta = 12.5$ and 5.4 mPa s. The maximum center velocity shows about the same values, but the profile of $\eta = 5.4$ mPa s is wider, indicating higher volume flow due to lower friction in the fluid. At lower viscosity the fluctuation levels for $u^2/u_{m,c}^2$ are higher in the shear layer, referring to more fluctuations thus more

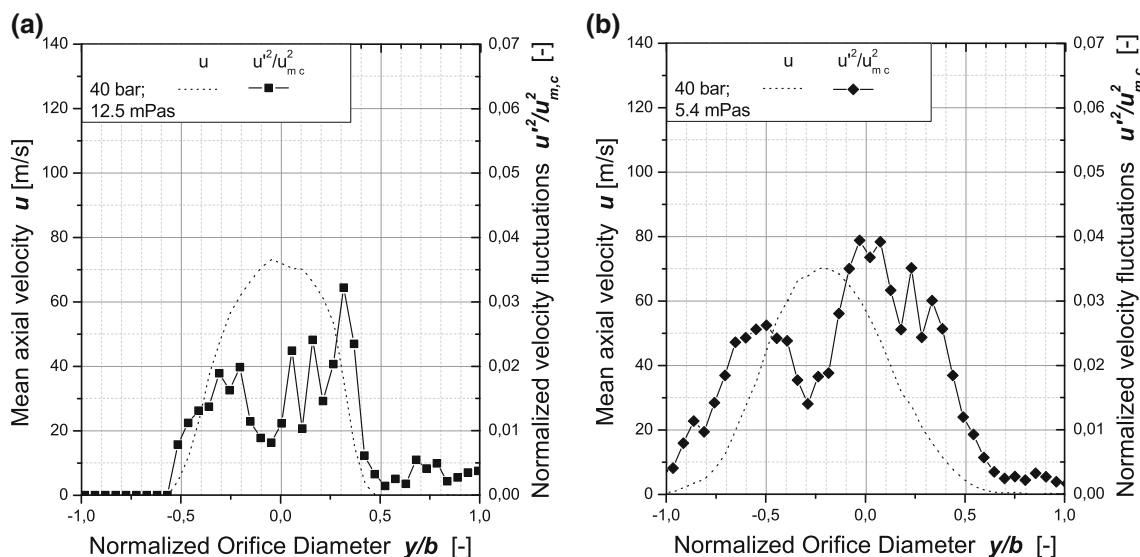
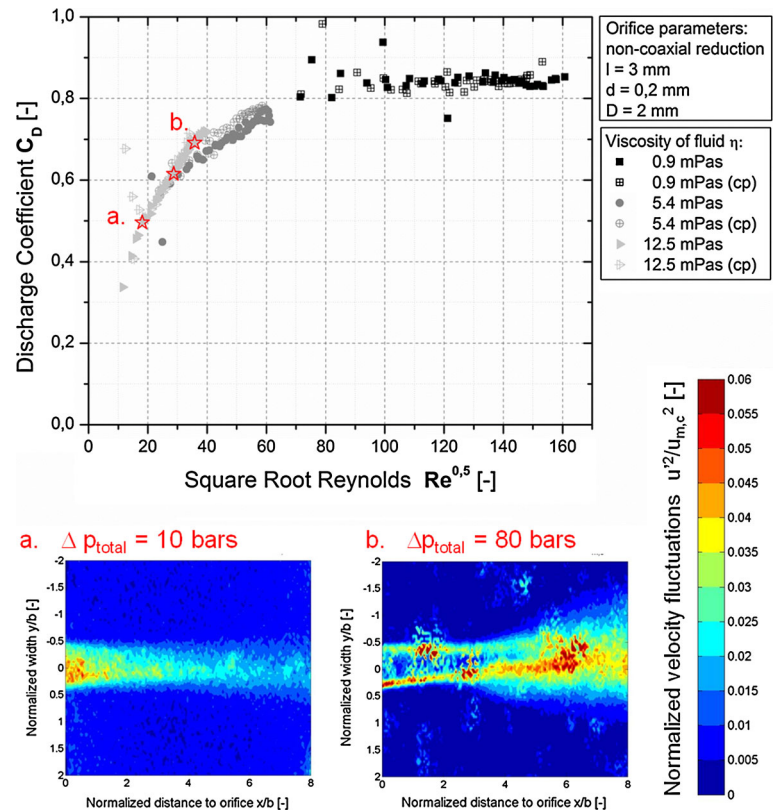


Fig. 13 Axial velocity u and normalized velocity fluctuations $u^2/u_{m,c}^2$ at a constant distance downstream of the orifice $x/b = 2.5$ at a constant homogenization pressure of $\Delta p_{\text{total}} = 40$ including counter pressure. **a** $\eta = 12.5$ mPa s **b** $\eta = 5.4$ mPa s

Fig. 14 Comparison between C_D measurements and μ PIV measurements



instabilities in the flow. Although not complete convergence was reached for all measurement regions and conditions in the flow fields, the μ PIV data show the developing laminar jet and arising instabilities in the shear layer in the jet at higher homogenization pressures and thus give valuable hints on the mechanisms that cause droplet breakup.

2.3 Comparison between the two measurement techniques

The flow visualization with μ PIV, the mean flow velocity fields and normalized fluctuation levels of $u'^2/u_{m,c}^2$ are in the following associated with the C_D measurements.

The three stars in Fig. 14 label the three process conditions ($\Delta p_{\text{total}} = 10, 40$ and 80 bars) where μ -PIV measurements were conducted. According to the literature, different flow regimes were determined from the C_D measurements by the following criteria:

Laminar flow: C_D value increases linear with $Re^{0.5}$ ($\Delta p_{\text{total}} = 10 \text{ bars}$)

Transitional flow: Slope of the C_D curves bends ($\Delta p_{\text{total}} = 40$ and 80 bars)

Turbulent flow: C_D value is independent of $Re^{0.5}$

The corresponding contours of the fluctuation levels for $\Delta p_{\text{total}} = 10$ and 80 bars are depicted in Fig. 14 as well.

The values estimated with both methods are in good compliance. In the region defined as laminar flow by the C_D

measurements, only small fluctuation levels could be detected and they strongly decreased shortly after the orifice.

In the region defined as transitional flow by the C_D measurements, μ PIV measurements showed instabilities in the shear layer of the jet which widens further downstream.

3 Conclusion

Characterizing and understanding local flow conditions in high pressure homogenization devices is crucial to control the droplet breakup and resulting droplet size distributions. However, the access of any inline measurement technique is challenging due to narrow tubes and high pressures during the process.

Two different measurement techniques to distinguish from laminar, transitional and turbulent flow conditions and quantify stresses behind a high pressure orifice were suggested and could be successfully applied in this investigation.

As an overall method, the characteristic correlation between the C_D value and $Re^{0.5}$ was used to describe the flow conditions. Two orifice units with varied axial position of the orifice showed the predicted characteristic course of the curve. Laminar and turbulent flow conditions could be distinguished by the curve.

Velocity fields at the outlet and at several positions downstream of the orifice up to $x/b < 50$ were measured

via μ PIV which was not possible in previous investigation due to available cameras. Mean velocities and fluctuation levels were calculated for the first time from these velocity fields. The amount of vectors valid for the calculations was about 60 % when applying counter pressure of about 15 %. Without counter pressure gas bubbles due to cavitation interfered with the measurement and led to a decrease of valid vectors to <40 %.

For the local flow investigations via μ PIV, only the optically accessible orifice unit was used, with a non-coaxial reduction next to the wall. The developing wall jet spread out behind the orifice showing a decrease at laminar conditions and a region where the velocity was uniform within at higher homogenization pressures. Further downstream the jet bents in z -direction and thus out of the measurement plane, which was parallel to the orifice.

In this region ($x/b < 2.5$), the normalized velocity fluctuations $u'^2/u_{m,c}^2$ were found to increase with rising Δp_{total} (rising Re , respectively) and lower viscosity.

At low *Reynolds* Numbers ($Re \leq 400$), the jet showed no instabilities at the outlet and a decreasing $u'^2/u_{m,c}^2$ at x/b between 2.5 and 8 indicating laminar flow conditions as predicted by the C_D measurements. At higher *Reynolds* Numbers, $u'^2/u_{m,c}^2$ peaks in the shear layers of the jet can be seen. These peaks spread out over radial position with increasing downstream coordinate.

A decrease in viscosity from 12.5 to 5.4 mPa s led to higher $u'^2/u_{m,c}^2$ at constant Δp .

With the setup used, the measurements were limited to the outlet of the orifice until $x/b < 8$. Further investigations will focus on the downstream area to prove at which conditions the jet turns laminar again or shows transition to completely turbulent conditions. For that reason, the number of PIV images needs to be increased. Additionally, the results conducted via μ PIV will be compared with an orifice with a co-axial reduction to eliminate the influences of the wall. Following investigations will focus on the use of these results to predict the deformation and breakup of droplets that are inserted in this fluid.

Acknowledgments This project is part of the JointLab IP3, a joint initiative of KIT and BASF. Financial support by the ministry of science, research and the arts of Baden-Württemberg (Az. 33-729.61-3) and the German research foundation (DFG) under the individual grants program KA 1808/8 and CI 185/3 is gratefully acknowledged.

References

- Armaly BF, Durst F, Pereira JCF, Schönung B (1983) Experimental and theoretical investigation of backward-facing step flow. *J Fluid Mech* 127:473–496
- Ball CG, Fellouah H, Pollard A (2012) The flow field in turbulent round free jets. *Prog Aerosp Sci* 50:1–26
- Blonski S, Korczyk PM, Kowalewski TA (2007) Analysis of turbulence in a micro-channel emulsifier. *Int J Therm Sci* 46(11):1126–1141
- Bogema M, Monkmeier PL (1960) The quadrant edge orifice—a fluid meter for low Reynolds numbers. *J Basic Eng* 82:729–734
- Brennen CE (1995) *Cavitation and bubble dynamics*, Oxford University Press, 0-19-509409-3
- Freudig B, Tesch S, Schubert H (2003) Production of emulsions in high-pressure homogenizers—Part II: influence of cavitation on droplet breakup. *Eng Life Sci* 6(3):266–270
- Galinat S, Torres LG, Masbernat O, Guiraud P, Risso F, Dalmazone C, Noik C (2007) Breakup of a drop in a liquid–liquid pipe flow through an orifice. *AIChE J* 53(1):56–68
- Gothsch T, Schilcher C, Beinert S, Richter C, Dietzel A, Büttgenbach S, Kwade A (2014) High-pressure microfluidic system (HPMS): flow and cavitation measurements in supported silicon microsystem. *Microfluid Nanofluidics*. doi:10.1007/s10404-014-1419-6
- Grace HP (1982) Dispersion phenomena in high viscosity immiscible fluid systems and application of static mixers as dispersion devices in such systems. *Chem Eng Commun* 14(3–6):225–277
- Hinze JO (1955) Fundamentals of the hydrodynamic mechanism of splitting in dispersion processes. *AIChE J* 1(3):289–295
- Hsiao FB, Lim YC, Huang JM (2010) On the near-field flow structure and mode behaviors for the right-angle and sharp-edged orifice plane jet. *Exp Therm Fluid Sci* 34(8):1282–1289
- Innings F, Trägårdh C (2007) Analysis of the flow field in a high-pressure homogenizer. *Exp Therm Fluid Sci* 32(2):345–354
- Innings F, Fuchs L, Trägårdh C (2011) Theoretical and experimental analyses of drop deformation and break-up in a scale model of a high-pressure homogenizer. *J Food Eng* 103(1):21–28
- Johansen FC (1930) Flow through pipe orifices at low Reynolds numbers. *Proc R Soc Lond A Math Phys Sci* 126(801):231–245
- Karbstein H (1994) Untersuchungen zum Herstellen und Stabilisieren von Öl-in-Wasser-Emulsionen, Dissertation, Universität Karlsruhe (TH)
- Keane RD, Adrian RJ (1990) Optimization of particle image velocimeters. 1. Double pulsed systems. *Meas Sci Technol* 1(11):1202–1215
- Kelemen K, Schuch A, Schuchmann HP (2014) Influence of flow conditions in high pressure orifices on droplet disruption of O/W emulsions. *Chem Eng Technol* 37(7):1227–1234
- Kolmogorov AN (1958) Über die Zerstäubung von Tropfen in einer turbulenten Strömung. In: Goering H (ed) *Sammelband zur statistischen Theorie der Turbulenz*. Akademie-Verlag, Berlin
- Lichtarowicz A, Duggins RK, Markland E (1965) Discharge coefficients for incompressible non-cavitating flow through long orifices. *J Mech Eng Sci* 7(2):210–219
- Mi J, Nathan GJ (2010) Statistical properties of turbulent free jets issuing from nine differently-shaped nozzles. *Flow Turbul Combust* 84(4):583–606
- Mi J, Kalt P, Nathan GJ, Wong CY (2007) PIV measurements of a turbulent jet issuing from round sharp-edged plate. *Exp Fluids* 42(4):625–637
- Milanovic IM, Hammad KJ (2010) PIV Study of the near-field region of a turbulent round jet, 3rd Joint US-European Fluids Engineering Summer Meeting and 8th International Conference on Nanochannels, Microchannels, and Minichannels
- Olsen MG, Adrian RJ (2000) Out-of-focus effects on particle image visibility and correlation in microscopic particle image velocimetry. *Exp Fluids* 29:S166–S174
- Pai S-I (1954) *Fluid dynamics of jets*. D. van Nostrand Company Inc, Toronto
- Reynolds O (1883) An experimental investigation of the circumstances which determine whether the motion of water shall be

- direct or sinuous, and of the law of resistance in parallel channels. *Philos Trans R Soc Lond* 174:935–982
- Rossi M, Segura R, Cierpka C, Kahler CJ (2012) On the effect of particle image intensity and image preprocessing on the depth of correlation in micro-PIV. *Exp Fluids* 52(4):1063–1075
- Santiago JG, Wereley ST, Meinhart CD, Beebe DJ, Adrian RJ (1998) A particle image velocimetry system for microfluidics. *Exp Fluids* 25(4):316–319
- Schlichting H (1933) Laminare Strahlausbreitung. *Z Angew Math Mech* 13(4):260–263
- Singh G, Sundararajan T, Bhaskaran KA (2003) Mixing and entrainment characteristics of circular and noncircular confined jets. *J Fluids Eng* 125(5):835–842
- Stang M, Schuchmann HP, Schubert H (2001) Emulsification in high-pressure homogenizers. *Eng Life Sci* 4(1):151–157
- Tihon J, Penkavova V, Havlica J, Simcik M (2012) The transitional backward-facing step flow in a water channel with variable expansion geometry. *Exp Therm Fluid Sci* 40:112–125
- Tollmien W (1926) Berechnung turbulenter Ausbreitungsvorgänge. *Z Angew Math Mech* 6(6):468–478
- Tunay T, Sahin B, Akilli H (2004) Investigation of laminar and turbulent flow through an orifice plate inserted in a pipe. *Trans Can Soc Mech Eng* 28(2B):403–414
- Vennemann P, Kiger KT, Lindken R, Groenendijk BCW, Stekelenburg-de Vos S, ten Hagen TLM, Ursem NTC, Poelmann RE, Westerweel J, Hierck BP (2006) In vivo micro particle image velocimetry measurements of blood-plasma in the embryonic avian heart. *J Biomech* 39(7):1191–1200
- Wolf F, Schuch A, Köhler K, Schuchmann HP (2012) Ansatz zur Beschreibung der zerkleinerungsrelevanten Strömungsverhältnisse beim Emulgieren von W/O-Emulsionen mit Lochblenden. *Chem Ing Tech* 84(12):2215–2220. doi:[10.1002/cite.201100065](https://doi.org/10.1002/cite.201100065)